Vaporisation of Water Droplets in a Laminar Gas Boundary Layer

D Esterhuyse [1] and D. G. Kröger [2]

A theory is developed for two-phase flow where water droplets in a gas stream penetrate a boundary layer. This theory is developed in order to determine the trajectory of different sized droplets in the boundary layer and to determine the improvements in heat transfer rate as a result of the evaporation of the droplets. The equations of motion of the droplets are derived for both a horizontal configuration and a vertical configuration and a model is derived for determining the heat transfer rate. The theory is applied to calculate droplet trajectories and enhancements in heat transfer rate for the surface of a fin tube heat exchanger. The results indicated that even droplets of very small size will impact the fin surface rapidly, while a horizontal plate will experience less wetting. The heat transfer calculations showed a marked improvement in heat transfer (up to 77%) with the introduction of droplets into the boundary layer.

NOMENCLATURE

A integration constant (dimensionless)
a area (m^2)
B integration constant (dimensionless)
b width (m)
C parameter defined by equation (16)
D binary vapor diffusivity ($m^2 \cdot s^{-1}$)
d diameter (m)
F force (N)
g acceleration due to gravity ($m \cdot s^{-2}$)
h heat transfer coefficient ($W \cdot m^{-2} \cdot K^{-1}$)
$\overline{h}$ average heat transfer coefficient in absence of droplets ($W \cdot m^{-2} \cdot K^{-1}$)
h_{fg} latent heat of vaporisation ($J \cdot kg^{-1} \cdot K^{-1}$)
K parameter defined by equation (21)
k thermal conductivity W ($\cdot m^{-1} \cdot K^{-1}$)
l length (m)
M molecular weight of water
$\overline{M}$ average molecular weight of boundary layer (air and water combined)
m mass (kg)
$\dot{m}''$ mass flux ($kg \cdot s^{-1} \cdot m^{-2}$)
Nu Nusselt number (dimensionless)
Pr Prandtl number (dimensionless)
p penetration (m), pressure ($N \cdot m^{-2}$)
q_t transverse velocity ($m \cdot s^{-1}$)
$\dot{q}''$ heat flux ($W \cdot m^{-2}$)
R resistance ($K \cdot W^{-1}$)
Re Reynolds number (dimensionless)
r radius (m)
Sh Sherwood number (dimensionless)
s spacing between adjacent fins (m)
T temperature (K)
t time (s)
u x-direction velocity ($m \cdot s^{-1}$)
v y-direction velocity ($m \cdot s^{-1}$)
x distance coordinate (m)
y distance coordinate (m)

Greek symbols

α parameter defined by equation (9) ($m^2 \cdot s^{-1}$)
β parameter defined by equation (10) ($m \cdot s^2$)
δ boundary layer thickness (m)
λ parameter defined by equation (5) ($m^2 \cdot s^{-1}$)
μ dynamic viscosity ($kg \cdot m^{-1} \cdot s^{-1}$)
ν kinematic viscosity ($m^2 \cdot s^{-1}$)
θ angle (deg)
ρ density ($kg \cdot m^{-3}$)
ξ point of entry of the droplet in the boundary layer (m)

Subscripts

a air
av average
bl boundary layer
eq equivalent
i interface, initial
l liquid
R relative, resultant
s droplet surface
t transverse
V vertical
∞ free stream conditions
0 surface, initial

1 Introduction

From an environmental perspective air-cooled industrial heat exchanger (ACHE) systems have the advantage of using less water than similar heat exchangers using wet cooling. Because of this ACHE systems are well suited for the use in industrial facilities situated in dry regions with limited water supply. The fact that these systems use less water, however, causes them to become inefficient during times of high ambient temperatures. Data on seasonal temperature fluctuations are available for most regions, but because of the high capital investment required for such a system, the ACHE will be designed for statistically averaged yearly temperatures and not necessarily for maximum temperatures. When the ACHE operates at maximum load during times of ambient temperatures higher than design values, the cooling capacity is reduced which in turn leads to decreased production of the associated facility.

The idea of improving the performance of an air-cooled heat exchanger by injection of liquid droplets into the gas stream and obtaining a liquid film, which displaces the gas boundary layer

[1] Msc.Ing. Mechanical Student, Stellenbosch University; Joubert Street 8, Stellenbosch.
[2] Professor, Department of Mechanical Engineering; University of Stellenbosch

from the solid surface, was first suggested by Elperin[1]. This type of spray cooling, whereby the heat exchanger surface is wetted, can be termed deluge cooling. Favorable results by Elperin[1] lead to other research on single cylinders and finned tubes[2,3]. The general trend of all the results was a marked increase in overall heat transfer.

Concerns over corrosion[4], fouling[5] and increased pressure drop as a result of fin congestion[6] prompted research into the use of a very fine water spray for precooling, termed fogging, whereby the droplets have evaporated before they reach the heat exchanger surface. This has the effect of reducing the drybulb temperature of the inlet air and enhancing the air side heat transfer as a result of evaporation of the droplets without wetting the surface of the heat exchanger. The latter effect, namely the enhancement of the air side heat transfer rate, is the focus of this study. A detailed investigation into the trajectories of droplets entering boundary layers formed on flat plates will be made as well as an investigation into the improvement of heat transfer coefficient with the evaporation of droplets in a boundary layer.

2 Analysis

2.1 Horizontal configuration

This analysis is based on the work done by Bhatti and Savery[7] on the augmentation of heat transfer in a laminar external gas boundary layer by the vaporisation of suspended droplets, with some variations in the droplet penetration equations. The equations of motion are derived for liquid droplets penetrating the hydrodynamic gas boundary layer on a flat surface and vaporising therein. Stoke's drag, buoyancy, and gravitational forces are taken into account. For this particular plate configuration, the force on the droplet due to its rotation was found to have a negligible effect and was therefore omitted from the model.

The following assumptions are made:

- The flow in the two-component, two-phase stream is laminar, steady, incompressible, and involves Newtonian fluids with constant properties.
- A linear velocity profile is assumed across the boundary layer. This assumption will be explained in more detail at the appropriate point in the analysis.
- The droplets obey Stoke's law and therefore the analysis is applicable to droplets with Reynolds number less than unity.
- The velocity and temperature of the droplets in the free stream are the same as those of the gas phase. This implies that the gas is saturated with liquid vapor.

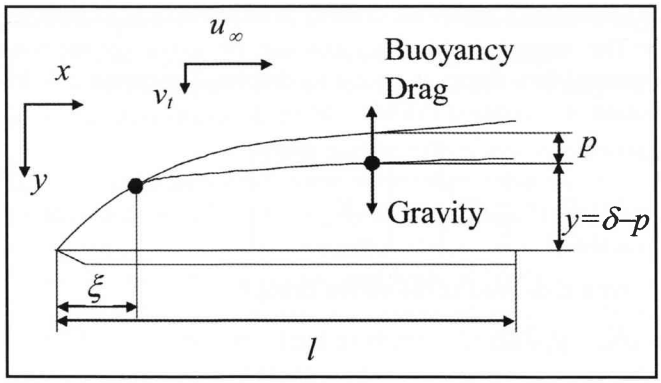

Figure 1: Schematic of the trajectory of a liquid droplet in a gas boundary layer

- Radiation effects are ignored.
- There is no temperature gradient in die droplets.
- The transverse velocity component of the laminar gas boundary layer is ignored.
- The free stream turbulence is isotropic and the level of the turbulence is relatively small. The laminar boundary layer therefore remains unaffected.
- The plate temperature is constant.

Transverse direction equation of motion

A water droplet entering a boundary layer on a flat plate is shown in figure 1. The forces acting on the droplet in the transverse direction are gravity (downwards) and the buoyancy force and drag force (upwards).

According to Newton's second law of motion

$$\frac{d}{dt}\left(m\frac{dp}{dt}\right) = mg - mg\left(\frac{p}{p_l}\right) - 6\pi\mu r\frac{dp}{dt} \qquad (1)$$

Express m in terms of r, simplify and rearrange

$$\frac{d^2p}{dt^2} + \left(\frac{3}{r}\frac{dr}{dt} + \frac{9\mu}{2\rho_l r^2}\right)\frac{dp}{dt} = \left(1 - \frac{p}{p_l}\right)g \qquad (2)$$

The vaporisation rate is used to determine the variation of droplet size with time [8]

$$\frac{dm}{dt} = \frac{2\pi r M\rho DSh}{\overline{M}}\ln\left(\frac{1-Y_\infty}{1-Y_0}\right) \qquad (3)$$

Express m in terms of r

$$\frac{dr}{dt} = \frac{1}{2r}\left[\frac{M\rho}{\overline{M}\rho_l}DSh\ln\left(\frac{1-Y_\infty}{1-Y_0}\right)\right] \qquad (4)$$

The Sherwood number, Sh, and the mole fractions Y_∞ and Y_o vary with time. However, if suitable average values are taken for Sh, Y_∞ and Y_o, the varying bracketed quantity in equation (4) can be set equal to a constant. In this manner a simple expression can be obtained for the variation of droplet radius with time. Thus, defining a parameter, λ

$$\lambda = \frac{1}{2}\left[\frac{M\rho}{\overline{M}\rho_l}DSh\ln\left(\frac{1-Y_\infty}{1-Y_0}\right)\right] \qquad (5)$$

Equation (4) now assumes the form

$$\frac{dr}{dt} = \frac{\lambda}{r} \qquad (6)$$

Integrating this equation and using the boundary condition at $t = 0, r = r_0$ yields

$$r^2 = r_0^2 = 2\lambda t \qquad (7)$$

Substituting equation (7) into equation (2) yields

$$\frac{d^2p}{dt^2} + \frac{1}{r^2}\left(3\lambda + \frac{9\mu}{2\rho_l}\right)\frac{dp}{dt} = \left(1 - \frac{p}{p_l}\right)g \qquad (8)$$

In this equation the quantities in the parentheses are constants and can be defined by the parameters a and β as

$$\alpha = \left(3\lambda + \frac{9\mu}{2\rho_l}\right) \tag{9}$$

and

$$\beta = \left(1 - \frac{p}{p_l}\right)g \tag{10}$$

Equation (8) now assumes the following form

$$\frac{d^2p}{dt^2} + \frac{\alpha}{r_0^2 + 2\lambda t}\frac{dp}{dt} = \beta \tag{11}$$

This equation is a second order linear differential equation with variable coefficients. It has the following solution

$$p = A(r_0^2 + 2\lambda t)^{(1-\alpha/2\lambda)} + B + \frac{\beta(r_0^2 + 2\lambda t)^2}{4\lambda(\alpha + 2\lambda)} \tag{12}$$

Evaluating the integration constants A and B with the following two boundary conditions: at $t = 0$, $p = 0$ and $\frac{dp}{dt} = v_t$ yields

$$A = \left[\frac{\beta r_0^2}{\alpha + 2\lambda} - v_t\right]\frac{r_0^{\alpha/\lambda}}{(\alpha - 2\lambda)} \tag{13}$$

$$B = -r_0^2\left[\frac{\beta r_0^2}{(\alpha^2 + 4\lambda^2)} - \frac{v_t}{(\alpha - 2\lambda)} + \frac{\beta r_0^2}{4\lambda(\alpha + 2\lambda)}\right] \tag{14}$$

Having evaluated the constants A and B it is now possible to determine the penetration of the water droplet into the boundary layer with equation (12). Bhatti and Savery[7] suggested that the contribution of the first term on the right-hand side of equation (12), $A(r_0^2 + 2\lambda t)^{(1-\alpha/2\lambda)}$, is negligible. They argued that because λ is numerically small and negative, it renders A vanishingly small. This is however not the case. Because λ is numerically small and negative, it results in A becoming extremely large (in the range of $1{\cdot}10^{251}$). The $(r_0^2 + 2\lambda t)^{(1-\alpha/2\lambda)}$ part of the term, however, becomes extremely small (in the range of $1{\cdot}10^{-256}$). The resultant product has indeed an influence on the equation.

By substituting the constants A and B back into equation (12), we now have an equation for the penetration of the droplet into the boundary layer at any time. By recalling that $y = \delta - p$, an equation can now be found for the transverse location of the droplet at any time

$$y = \delta_0 - A(r_0^2 + 2\lambda t)^{(1-\alpha/2\lambda)} + C - \frac{\beta(r_0^2 + 2\lambda t)^2}{4\lambda(\alpha + 2\lambda)} \tag{15}$$

where

$$C = r_0^2\left[\frac{\beta r_0^2 - 4\lambda v_t}{4\lambda(\alpha - 2\lambda)}\right] \tag{16}$$

Flow direction equation of motion

In 1908 Blasius[9] found a solution for the velocity profile in the boundary layer for laminar flow. However, accurate solutions for the Blasius equation have only been obtained by numerical integration. For the sake of mathematical simplicity, it was decided that a linear velocity profile in the boundary layer would be an adequate approximation

$$\frac{dx}{dt} = u_\infty\left(\frac{y}{\delta}\right) \tag{17}$$

The boundary layer thickness at any point along a flat plate is given by the equation by Blasius[9]

$$\delta = 5\left(\frac{\nu x}{u_\infty}\right)^{1/2} \tag{18}$$

Substituting equations (15) and (18) into equation (17), rearranging and inverting, yields an equation for the change in droplet exposure time with changing longitudinal position

$$\frac{dt}{dx} = \frac{5\nu^{1/2}x^{1/2}}{u_\infty^{3/2}\left[5\left(\frac{\nu}{u_\infty}\right)^{1/2}x^{1/2} - A\left(r_0^2 + 2\lambda t\right)^{\left(1-\frac{\alpha}{2\lambda}\right)} + C - \frac{\beta\left(r_0^2 + 2\lambda t\right)^2}{4\lambda(\alpha + 2\lambda)}\right]} \tag{19}$$

This differential equation can be solved using Euler's method or a Runge-Kutta method.

2.2 Vertical configuration

The equations of motion are derived for liquid droplets penetrating the hydro-dynamic gas boundary layer on a vertical flat surface and vaporising therein. For the vertical plate case, a significant force acting on the droplet in the horizontal plane is the force acting on the droplet due to rotation of the droplet, shown in figure 2. The rotation of the droplet is caused by the velocity profile in the boundary layer, resulting in the droplet experiencing a higher air velocity at its top than at its bottom.

The magnitude of this force can be found by applying potential flow theory to a rotating droplet. The pressure distribution on a rotating cylinder can by given as[10]

$$p - p_0 = \frac{1}{2}\rho u^2\left[1 - \left(\frac{2\sin\theta + \frac{K}{2\pi ur}}{}\right)\right] \tag{20}$$

with K defined as the vortex strength

$$K = q_t 2\pi r \tag{21}$$

A spherical droplet can be approximated as being made up of

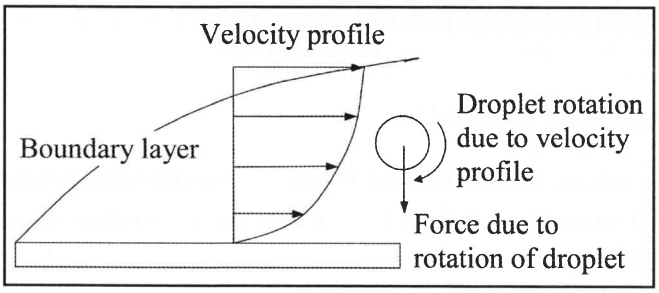

Figure 2: Schematic of the rotation of a droplet in a boundary layer caused by the velocity profile

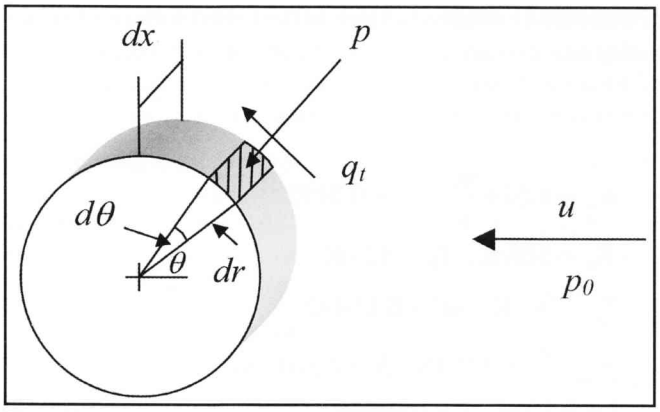

Figure 3: Pressure and velocity on the surface of a unit length of a cylinder

a large number of short cylinders of varying diameter. Figure 3 shows one such a cylinder.

The hatched area on the cylinder is the incremental area, *da*, and can be expressed as

$$da = d\theta \cdot dr \cdot dx \tag{22}$$

The resultant force on the cylinder therefore is

$$F_R = (p - p_o)d\theta \cdot dr \cdot dx \tag{23}$$

and the resultant vertical force is

$$F_V = (p - p_o)d\theta \cdot dr \cdot dx \sin\theta \tag{24}$$

Substituting equation (20) into equation (24) with $B = K/2\pi ur$ and integrating over the entire diameter of the sphere yields an equation for the vertical force on the droplet (F_V positive upwards)

$$F_V = -2\left[\int\int\int_0^{2\pi}\frac{1}{2}\rho u^2 \cdot \left(1-(2\sin\theta + B)^2\right)\sin\theta\, d\theta dr dx\right] \tag{25}$$

The first integral becomes

$$\int_0^{2\pi}\frac{1}{2}\rho u^2\left[\begin{matrix}\sin\theta(1-B^2)- \\ 4B\sin^2\theta - 4\sin^3\theta\end{matrix}\right]d\theta \tag{26}$$

which simplifies $4B\pi$ to upon integration. Completing the integration of equation (26) yields

$$F_V = 2\rho u^2 r^3 B\pi \tag{27}$$

Substituting the definitions of *B* and *K* into equation (27) yields an equation for the force on a droplet due to the rotation thereof

$$F_V = 2\rho u q_t r^3\pi \tag{28}$$

As in the horizontal flat plate model, free stream turbulence superimposed on the boundary layer is assumed to cause the initial transverse velocity component that propels the droplets towards the solid surface. The transverse and flow direction equations of motion are again solved simultaneously to obtain an expression for the exposure time of the droplets in the boundary layer. The same assumptions made for the flat plate model are applicable to this model, with the addition of the following assumptions:

- The tangential velocity of the droplet is equal to the difference in air velocity it experiences at the top and bottom of the droplet.
- The force on the droplet due to the rotation of the droplet is calculated using the boundary layer velocity at the droplet entry point.

Consider a water droplet entering a boundary layer formed on a vertical plate. The top view of this is shown schematically in figure 4. The gravity and buoyancy forces that acted on the droplet in the horizontal plate case are now absent. The forces acting on the droplet in the transverse direction consist of a force due to the rotation of the droplet and a drag force.

According to Newton's second law of motion

$$\frac{d}{dt}\left(m\frac{dp}{dt}\right) = 2\rho u_{bl} q_t r^3\pi - 6\pi\mu r\frac{dp}{dt} \tag{29}$$

Expressing *m* in terms of *r*, simplifying and rearranging yields

$$\frac{d^2p}{dt^2} + \left(\frac{3}{r}\frac{dr}{dt} + \frac{9\mu}{2\rho_l r^2}\right)\frac{dp}{dt} = \frac{3u_{bl}q_t}{2} \tag{30}$$

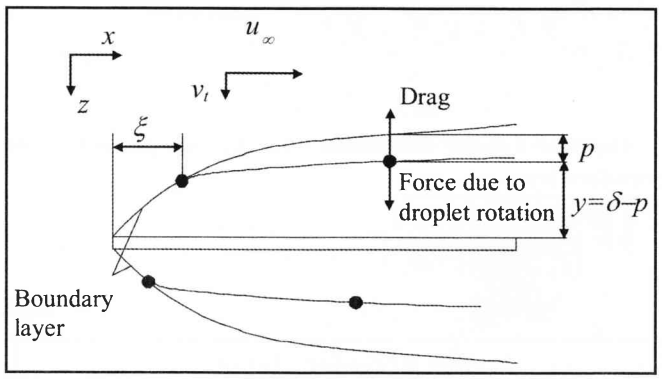

Figure 4: Schematic of a liquid droplet in a gas boundary layer formed on a vertical plate

This equation has the same form as equation (12), except that the parameter β is now defined as

$$\beta = \frac{3u_{bl}q_t}{2} \tag{31}$$

The same procedure that was followed for the horizontal plate model is now followed for the vertical plate model to determine the trajectories of droplets in the boundary layer.

2.3 Heat transfer coefficient enhancement

A simple two-region model was developed by Bhatti and Savery[7] for determining the heat transfer coefficient in the presence of droplets that penetrate and vaporise within the boundary layer. They define an outer region, where the heat transfer occurs by convection as well as by the vaporisation of the droplets, and an inner region, where no droplets occur and the heat transfer occurs by convection only. The boundary between the two regions is determined by the depth of penetration of the droplets into the boundary layer. In this analysis the depth of penetration is given by equation (12). The total resistance of the boundary layer can be divided into three resistances as shown in figure 5.

Bhatti and Savery[7] derived the following equations for the resistances R_1, R_2 and R_3

$$R_1 = \frac{1}{hbl}\left(\frac{\delta - p}{\delta}\right) \tag{32}$$

$$R_2 = \frac{1}{hbl}\left(\frac{p}{\delta}\right) \tag{33}$$

$$R_3 = K(T_i - T_\infty) \tag{34}$$

where

$$K = \frac{6m}{\Delta m \cdot \dot{m}'' sbh_{fg}} \tag{35}$$

and the interface temperature, T_i, is calculated with

$$T_i = \frac{K(R_1 T_\infty + R_2 T_0) - R_1 R_2}{K(R_1 + R_2)} \tag{36}$$

Knowing the resistances R_1, R_2 and R_3 from equations (32), (33) and (34), the total equivalent resistance of the boundary layer, R_{eq}, can be determined

$$R_{eq} = \frac{R_1 R_2 + R_2 R_3 + R_1 R_3}{R_2 + R_3} \tag{37}$$

The heat transfer coefficient with droplets present in the boundary layer is

$$h = \frac{\dot{q}''}{(T_0 - T_\infty)} = \frac{1}{R_{eq} bl} \tag{38}$$

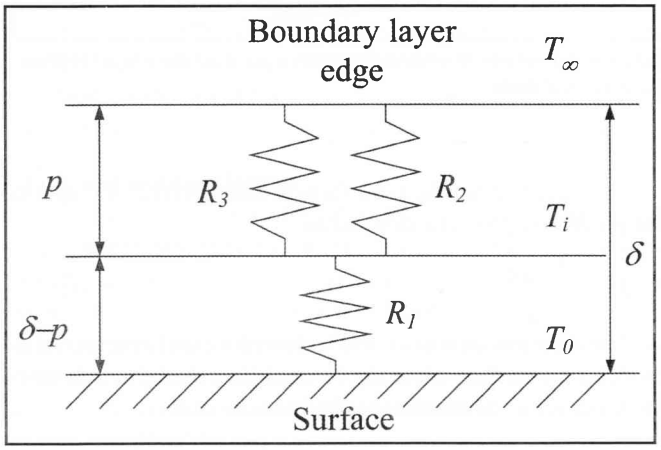

Figure 5: Schematic of the thermal resistance of a boundary layer

The average heat transfer coefficient for laminar flow, in the absence of droplets, can be found with the Pohlhausen[11] relation

$$Nu = \frac{\bar{h}l}{k} = 0.664\,\mathrm{Re}^{1/2}\,\mathrm{Pr}^{1/3} \tag{39}$$

with Re based on u_∞ and l. The ratio $\frac{h}{\bar{h}}$ gives the enhancement in heat transfer coefficient due to the vaporisation of the droplets.

3 Results and discussion

The use of the equations derived in the preceding section can be illustrated by applying them to the finned surface of an air-cooled heat exchanger. Test conditions similar to the ones used by Bhatti and Savery[7] in their analysis were used to make a comparison between the results easier. These conditions were

$$u_\infty = 1.524\,\frac{\mathbf{m}}{\mathbf{s}},\ v_t = 0.0152\,\frac{\mathbf{m}}{\mathbf{s}}$$

$$T_\infty = 308\,\mathbf{K},\ T_0 = 323\,\mathbf{K}$$

$$T_s = 291\,\mathbf{K},\ \dot{m}'' = 0.01492\,\frac{\mathbf{kg}}{\mathbf{m^2 s}}$$

$$p_{atm} = 101325\,\mathbf{Pa},\ b = 0.3048\,\mathbf{m}$$

$$l = 0.15\,\mathbf{m},\ s = 0.001\,\mathbf{m}$$

The physical properties used in the calculations are

$$M = 18\,\frac{\mathbf{kg}}{\mathbf{kg\ mole}},\ \overline{M} = 28\,\frac{\mathbf{kg}}{\mathbf{kg\ mole}}$$

$$\rho_l = 1001\,\frac{\mathbf{kg}}{\mathbf{m^3}},\ \rho_{av} = 1.25\,\frac{\mathbf{kg}}{\mathbf{m^3}}$$

$$\mu_a = 1.95 \cdot 10^{-5}\,\frac{\mathbf{kg}}{\mathbf{m \cdot s}}$$

$$\nu_a = 2.04 \cdot 10^{-5}\,\frac{\mathbf{m^2}}{\mathbf{s}}$$

$$D = 2.29 \cdot 10^{-5}\,\frac{\mathbf{m^2}}{\mathbf{s}}$$

$$k = 0.034\,\frac{\mathbf{W}}{\mathbf{m \cdot K}},\ h_{fg} = 2.4 \cdot 10^{6}\,\frac{\mathbf{J}}{\mathbf{kg}}$$

$$Sh_{av} = 2.59,\ r = 22.5 \cdot 10^{-6}\,\mathbf{m}$$

3.1 Droplet trajectory—horizontal configuration

Figure 6 shows the trajectory of droplets of 10 μm, 30 μm and 50 μm diameter in a laminar boundary layer on a flat plate. All the droplets enter the boundary layer at the same point: $\xi = 0.01$ m. From the figure it can be seen that for the 50 μm diameter droplet, the gravitational force dominates the buoyancy force. The droplet follows a trajectory that impacts the surface. The 30 μm diameter droplet curves towards the surface, but as the droplet becomes smaller, due to evaporation of the liquid, the buoyancy force becomes dominant, forcing the droplet upwards. The droplet evaporates before it has reached the surface. For the 10 μm diameter droplet the buoyancy and drag forces balance the gravitational force and it travels on a straight path. Because of the small size of the droplet, it evaporates rapidly.

Figure 7 shows the trajectories of a 40 micron diameter droplet entering the boundary layer at different points. It is apparent that as the entry point moves farther from the leading edge into the

thicker part of the boundary layer, the droplet experiences more evaporation. As the droplet becomes smaller, the buoyancy and drag forces become dominant over the gravitational force. At the entry point $\xi = 30$ mm, the droplet does not impact the surface.

It was found that droplets entering the boundary layer formed on the bottom of the plate follow similar trajectories as the droplets entering the top boundary layer. None of the droplets entering the bottom boundary layer will therefore impact the surface of the plate. These predictions are confirmed by experiments preformed by Bhatti and Savery[7].

3.2 Droplet trajectory – vertical configuration

Calculations were first performed to determine the trajectories of droplets of the same size (30 micron) entering the boundary layer formed on a vertical plate at different longitudinal distances on the plate. The results of the calculations are shown in figure 8.

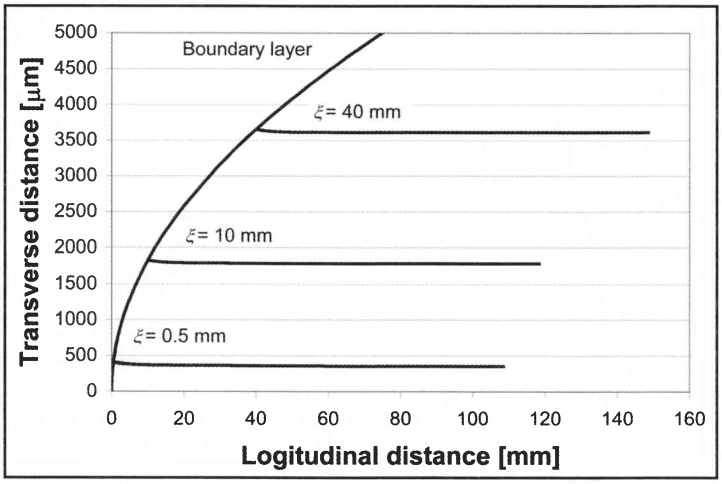

Figure 8: Trajectory of droplets entering a boundary layer on a vertical plate at different longitudinal distances

The graph shows the trajectories of the droplets as well as the point where the droplets have been completely vaporised. It can be seen that the force due to the rotation of the droplets and the drag force, both being relatively small forces, have only a small effect on the droplets. As the droplets enter the boundary layer, they start to spin in a clockwise direction (relative to the graph shown) as a result of the velocity profile. This results in a downward force on the droplets, forcing them towards the surface.

Once the droplets start to move, a drag force is exercised in the upward direction, resulting in smaller resultant force acting towards the surface. The droplet then moves toward the surface at a very slow rate, and is vaporised before it has impacted the surface. This will be the case for all droplets except those that enter extremely near to the leading edge of the plate.

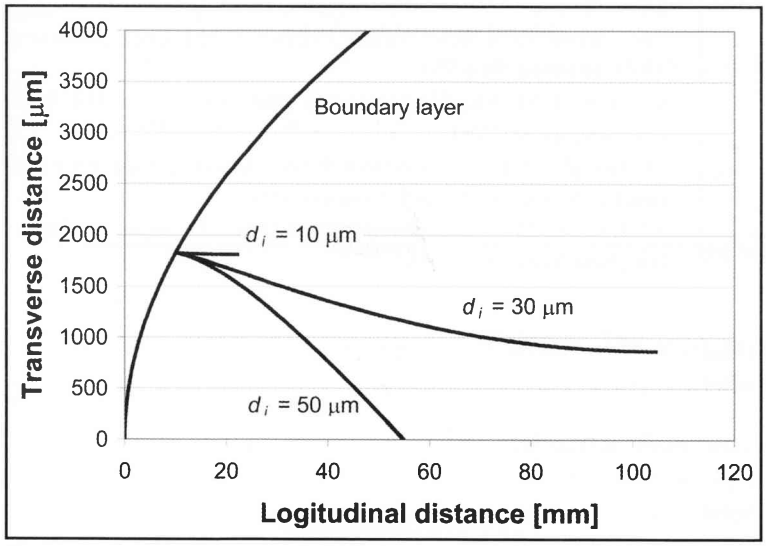

Figure 6: Trajectory of different sized droplets entering a boundary layer on a horizontal plate

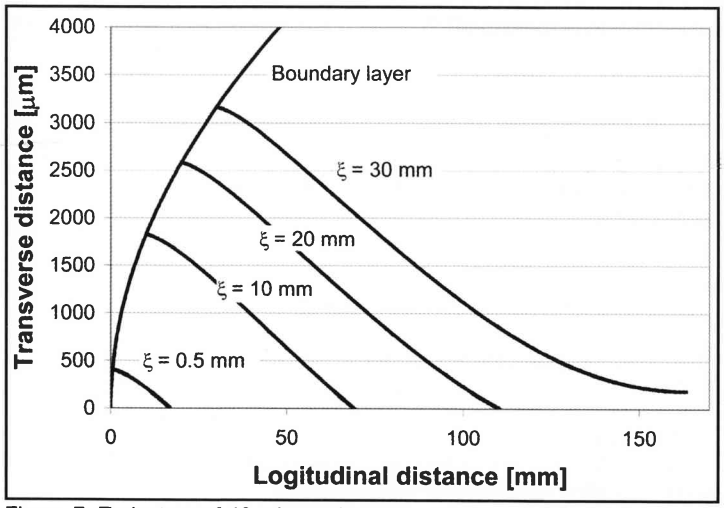

Figure 7: Trajectory of 40 micron droplets entering a boundary layer on a horizontal plate

Calculations were also performed for droplets of different diameter entering the boundary layer at the same point ($\xi = 0.01$ m). The results of these calculations are shown in figure 9. This graph shows that the as the droplet becomes larger, it experiences a bigger force towards the surface. A possible explanation for the phenomenon is that the larger droplets experience a higher rate of rotation and therefore a larger downward force.

This higher rate of rotation is as a result of the bigger difference in velocities that the droplet experiences at its top and bottom.

3.3 Heat transfer calculations

Figure 10 shows the calculations described above performed for different droplet diameters and droplet mass fluxes on a vertical plate. The calculations are identical for a horizontal plate configuration. It can be seen that for constant droplet mass fluxes, the larger diameter droplets cause greater enhancement in the heat transfer coefficient. This greater enhancement is due to greater evaporation rates, which result from increased exposure time and penetration of the larger-sized droplets. The figure also shows that as the droplet mass flux in the main stream increases, the enhancement for the same diameter droplet also increases.

This is to be expected, since the increase in droplet flux implies that a greater number of droplets are available for evaporation.

For the largest mass flux, $\dot{m}$"0.04069 kg/m^2s and a droplet diameter of 45 μm, a heat transfer enhancement of 77% is achieved. This constitutes a major improvement in heat transfer, and although this mathematical model is only

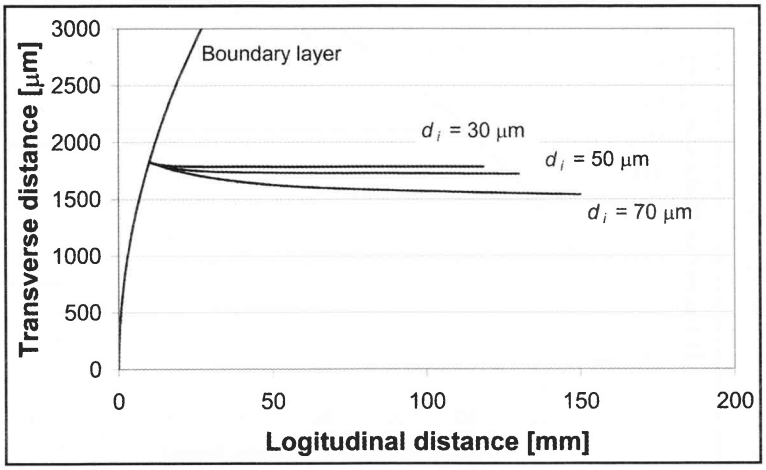

Figure 9: Trajectories of different sized liquid droplets entering a boundary layer on a vertical plate at the same point

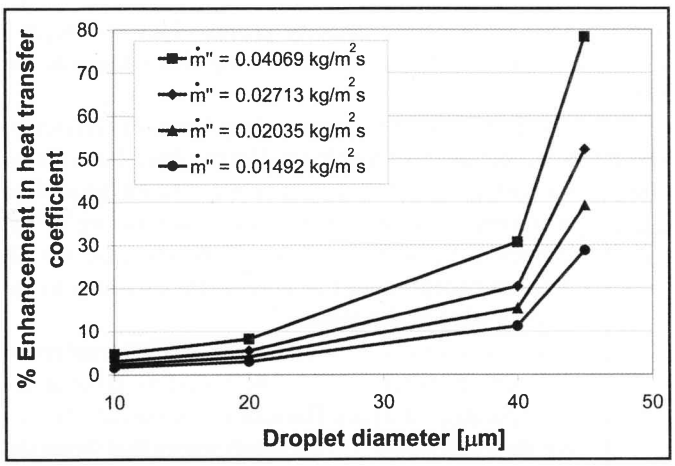

Figure 10: Dependence of the heat transfer on the droplet diameter and mass flux

representative of the idealised case, if anything close to this improvement could be achieved in practice this would have major benefits.

4 Conclusion

Mathematical models were derived for the trajectories of liquid droplets in hydrodynamic boundary layers formed on flat plates. Models were derived for a vertical as well as a horizontal plate configuration. A model was also derived to determine the improvement in heat transfer coefficient with droplets evaporating in the boundary layer.

Comparing the droplet trajectories of the horizontal plate model with the vertical plate model, it can be seen that for the case where the fins of a heat exchanger are vertical, the droplets experience a reduced force towards the surface. This is due to the fact that the large influence of gravity that is present in the horizontal plate model is absent in the vertical plate model. This indicates that heat exchangers with vertical fin configurations would experience reduced surface wetting if droplets of sufficiently small size are used to cool the heat exchanger. Significant improvements in the heat transfer coefficient are found when droplets are evaporated in the boundary layer.

References

1. Elperin I.T. *Heat Transfer of Two-Phase Flow with a Bundle of Tubes,* Inzhererno Fizicheski Zhurnal, 1961, 4 (8) pp. 30-35.

2. Nakayama W., Kuwahara H., Hirasawa S. *Heat transfer from tube banks to air/water mist flow,* International Journal of Heat and Mass Transfer, 1988, 31 (2) pp. 449-460.

3. Lee S.L., Yang Z.H., Hsyua Y., *Cooling of a heated surface by mist flow,* Journal of Heat Transfer, 1994, 116 pp. 167-172.

4. Woest M., Hearn I., Lennon S.J., *Investigation into the corrosion behavior of galvanized finned tubing for cooling under deluge enhanced wet/dry cooling conditions,* ESCOM, Scientific Investigations Report No. S91/030, 1991.

5. Leidenfrost W., Korenic B., *Evaporative cooling and heat transfer augmentation related to reduced condenser temperatures,* Heat Transfer Engineering, 1982, 3 (3-4) pp. 38-59.

6. Kriel D.E., *Prediction and measurement of the performance of spray cooled heat exchangers,* M.Eng Thesis, University of Stellenbosch, 1991.

7. Bhatti M.S., Savery C.W., *Augmentation of heat transfer in a laminar external gas boundary layer by the vaporisation of suspended droplets,* Journal of Heat and Mass Transfer, May 1975, pp. 179-184.

8. Savery C.W., Juedes D.L., Borman G.L., n-Heptane, *Carbon Dioxide and Chlorotrifluoromethane Droplet Vaporisation Measurements at Supercritical Pressures,* Ind. Chem. Fundam, 1971, 10 (4) pp. 543-553.

9. White F.M., *Fluid Mechanics,* 4th edition, McGraw-Hill Book Co., Singapore, 1994.

10. Houghton, E. L., Carpenter, P. W., Aerodynamics for Engineering Students, Arnold, London, 1993.

11. Kays W.M., *Convective Heat and Mass Transfer,* McGraw-Hill, New York, 1966.